Nitrogen-doped graphene nanosheets as cathode materials with excellent electrocatalytic activity for high capacity lithium-oxygen batteries

Yongliang Li, Jiajun Wang, Xifei Li, Dongsheng Geng, Mohammad N. Banis, Ruying Li, Xueliang Sun *

Department of Mechanical and Materials Engineering, University of Western Ontario, 1151 Richmond Street N., London, Ontario, Canada N6A 5B9

ARTICLE INFO

ABSTRACT

Nonaqueous lithium-oxygen battery with nitrogen-doped graphene nanosheets (N-GNSs) as cathode materials delivered a discharge capacity of 11660 mAh g^{-1}, which is about 40% higher than that with the pristine graphene nanosheets (GNSs). The electrocatalytic activity of N-GNSs for oxygen reduction in the nonaqueous electrolyte is 2.5 times as that of GNSs. The excellent electrochemical performance of N-GNSs is attributed to the defects and functional groups as active sites introduced by nitrogen doping.

© 2012 Elsevier B.V. All rights reserved.

1. Introduction

Nonaqueous lithium-oxygen/air batteries have great potential for electric vehicles (EVs) and hybrid electric vehicles (HEVs) due to their extremely high energy density [1,2]. The air electrode plays an important role in the battery performance; however, it is still a critical challenge to develop an optimum carbon cathode with appropriate surface area, porosity and morphology [3–5].

Graphene nanosheets (GNSs) have been reported as ideal cathode materials for lithium-oxygen batteries because of their unique morphology and structure which provide both diffusion channels for O_2 and active sites for cathode reactions [6–8]. Chemical doping with nitrogen atoms into GNSs can modify the electronic property, provide more active sites, and enhance the interaction between carbon structure and other molecules, thus improve the performance in various applications, such as fuel cells, lithium-ion batteries, supercapacitors, etc [9–11].

Recent studies reported that nitrogen-doped carbon powder and carbon nanotubes showed higher discharge capacities than the pristine counterparts, however, there is no report on nitrogen-doped graphene nanosheets (N-GNSs) as cathode materials for lithium-oxygen batteries [12,13]. In this study, for the first time, N-GNSs were employed in lithium-oxygen batteries, and it was found that they show excellent electrocatalytic activity for oxygen reduction, therefore, increasing about 40% of the discharge capacity compared to GNSs. This finding not only shows that N-GNSs are promising electrode materials, but also gives a rational direction to modify other carbon materials for application in lithium-oxygen batteries.

2. Experimental

2.1. Materials synthesis

GNSs were prepared by the oxidation of graphite powder using the modified Hummers' method, and N-GNSs were prepared by post heating the GNSs under high purity ammonia mixed with Ar at 900 °C for 5 min [10,11].

2.2. Physical characterizations

Morphology of GNSs and N-GNSs and discharge products were characterized by a Hitachi H-7000 TEM and a Hitachi S-4800 FESEM, respectively. XRD patterns were recorded by a Bruker-AXS D8 Discover diffractometer (Co-Kα source). XPS spectra were tested by a Kratos Axis Ultra X-ray photoelectron spectrometer (Al Kα source). Raman scattering spectra were recorded on a HORIBA Scientific LabRAM HR system (532.4 nm laser). N_2 adsorption/desorption isotherms were obtained using a Folio Micromeritics TriStar II Surface Area and Pore Size Analyzer.

2.3. Electrochemical measurements

Swagelok type cells were used to test the battery performance. GNSs or N-GNSs and PVDF (Alfa Aesar) with a weight ratio of 9:1 were casted onto a separator (Celgard 3500) and cut to 3/8 in. in diameter as cathodes and the material loadings were ~0.3 mg. 1 mol dm^{-3} LiPF$_6$ in

---

* Corresponding author. Tel.: +1 519 6612111x87759; fax: +1 519 6613020.
E-mail address: xsun@eng.uwo.ca (X. Sun).

tetraethylene glycol dimethyl ether (TEGDME) was used as electrolyte. The discharge/charge characteristics were performed by using an Arbin BT-2000 battery station in a voltage range of 2.0–4.5 V in a 1 atm oxygen atmosphere at 25 °C.

The cyclic voltammetry (CV) tests were conducted in a three-electrode cell. A platinum wire was used as the counter electrode. A silver wire immersed into 0.1 mol dm^{-3} AgNO$_3$ in TEGDME solution, connected to the main solution by a glass frit, was used as reference electrode. A glass carbon disk (0.196 cm^2, Pine Inc.) covered by 10 μL of the suspension made with 2 mg of GNSs or N-GNSs and 2 mg of PTFE (Sigma-Aldrich) in a 30% 2-propanol/water solution was used as the working electrode. CV curves were recorded by scanning the disk potential from 3.5 to 2.0 V (0.1 mol dm^{-3} LiPF$_6$/TEGDME) at a scan rate of 5 mV s^{-1} by using an Autolab Potentiostat/Galvanostat (PGSTAT-30, Brinkmann Instruments) at 25 °C.

3. Results and discussion

As shown in Fig. 1a, the initial discharge capacity of GNSs electrode is 8530 mAh g^{-1} at a current density of 75 mA g^{-1}, while 11,660 mAh g^{-1} for N-GNSs, which is about 40% higher than that of GNSs. With the current densities increase, the discharge capacities of both samples decrease, which are 5333 and 3090 mhA g^{-1} for GNSs and 6640 and 3960 mAh g^{-1} for N-GNSs at current densities of 150 and 300 mA g^{-1}, respectively. N-GNSs electrode not only exhibits higher discharge capacity but also shows higher average discharge plateau than GNSs electrode at various discharge current densities, indicating a higher catalytic activity for cathode reaction which may due to the higher binding energy of oxygen after nitrogen doping [14,15].

The cyclic voltammogram (CV) curves of GNSs and N-GNSs are shown in Fig. 1b. Featureless voltammetric currents were observed in the Ar-saturated solution (inset of Fig. 1b), while in the O$_2$-saturated solution, the onset potentials of oxygen reduction reaction (ORR) for GNSs and N-GNSs are at 2.76 V and 2.8 V, respectively. The positively shift of the onset potential and the great and well-defined enhanced reduction peak at 2.29 V of N-GNSs indicate a superior electrocatalytic activity for ORR. From the rotating disk electrode (RDE) voltammetry measurements, it can be seen that the onset potential of ORR for N-GNSs (2.84 V) is still positive shift compared to GNSs (2.79 V) (Fig. 1c). There is no well-defined diffusion limiting current plateau for both samples which is similar to other non-noble catalysts especially pure carbon for ORR, however, the current density of N-GNSs at 2 V is about 2.5 times as that of GNSs [16,17]. Furthermore, the numbers of electron transferred in ORR are 0.99 for N-GNSs and 0.80 for GNSs, respectively, according to the Tafel-slops shown in Fig. 1d [18]. These results also suggest that N-GNSs have higher catalytic activity for ORR in a nonaqueous solution than GNSs.

N-GNSs and GNSs show no obvious difference from the structure and morphology but the same micro/meso-porosity and pore size distribution (Fig. 2a, b and c). XPS confirms that three types of nitrogen (pyridinic-N, pyrrolic-N, and graphitic-N) are formed in N-GNSs and the nitrogen percentage is about 2.8 at.% (Fig. 2d). The structural defects introduced by nitrogen doping increases the amount of unsaturated carbon atoms (Fig. 2e); and these atoms are very active to react with oxygen and form oxygen-containing groups (C–O, C=O, and O=C–O), which can catalyze the ORR (Fig. 2f.) [19,20]. The Raman spectra of GNSs and N-GNSs are shown in Fig. 2g. The intensity ratio of D band (~1350 cm^{-1}) to G band (~1595 cm^{-1}) for GNSs and N-GNSs are 0.96 and 1.10, respectively, confirming that there are more
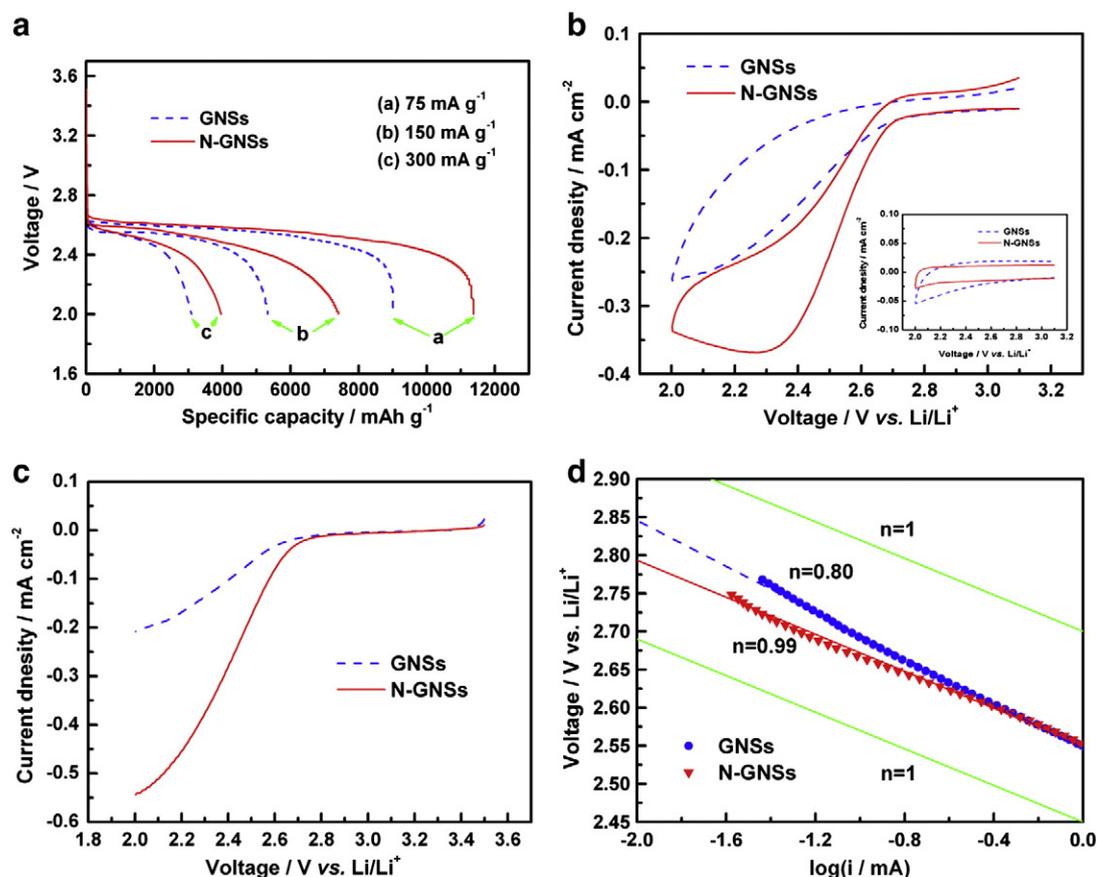
Fig. 1. a, Voltage profiles of GNSs and N-GNSs electrodes at various current densities; b, CVs of GNSs and N-GNSs electrodes in O$_2$-saturated 0.1 mol dm^{-3} LiPF$_6$ in TEGDME solution at a scan rate of 5 mV s^{-1}, inset is the CVs in Ar-saturated solution; c, rotating-disk electrode voltamograms recorded for GNSs and N-GNSs electrodes for ORR at a rotating speed of 100 rpm in O$_2$-saturated 0.1 mol dm^{-3} LiPF$_6$ in TEGDME solution at a scan rate of 5 mV s^{-1}; d, Tafel-slops for the ORR on the GNSs and N-GNSs electrodes.
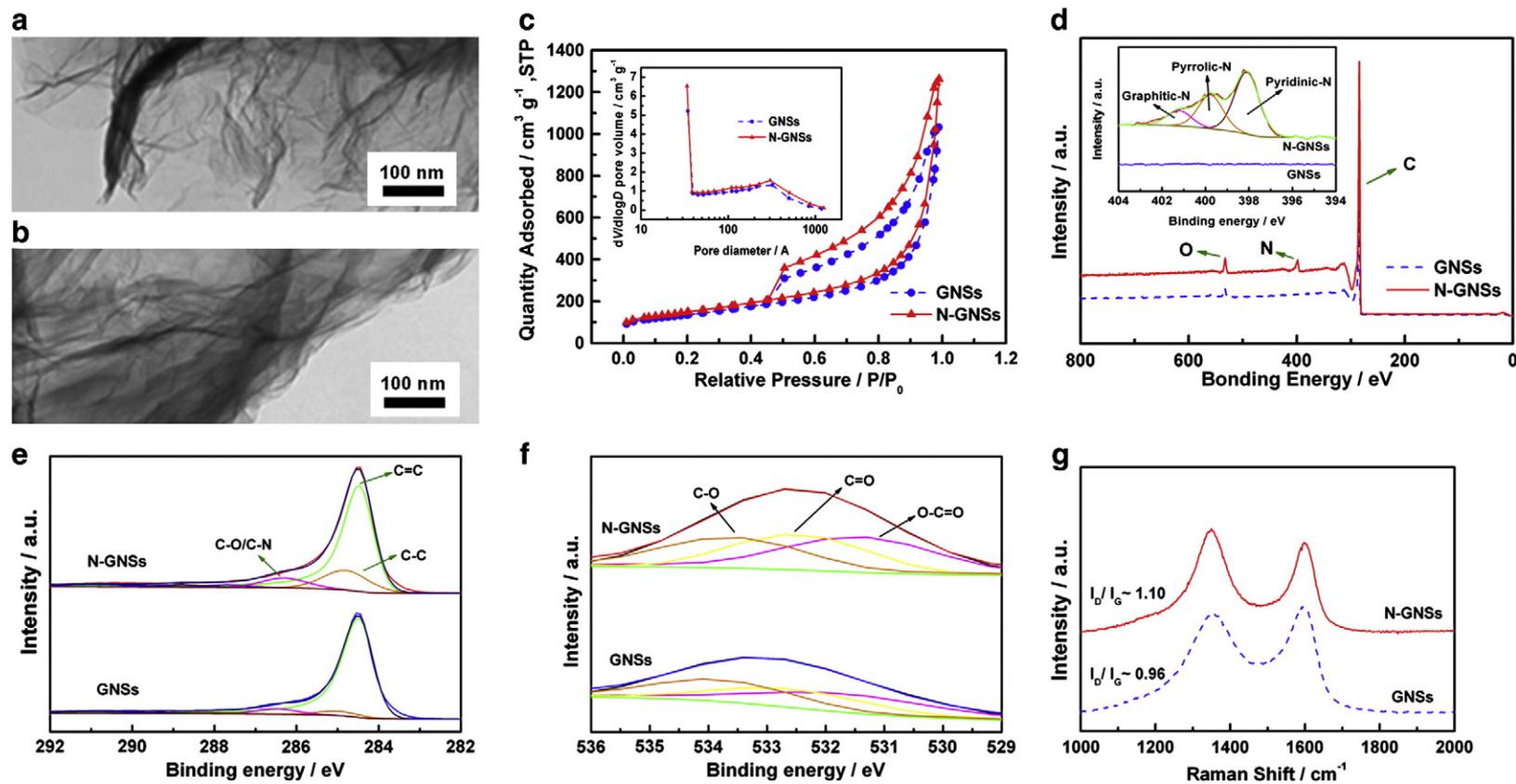
Fig. 2. TEM images of a, GNSs and b, N-GNSs; c, N_2 adsorption–desorption isotherms at 77 K, inset is the pore size distribution; XPS d, survey, e, C1s, and f, O1s spectra of GNSs and N-GNSs, inset of d is N 1s spectra of two samples; g, Raman spectra of GNSs and N-GNSs.
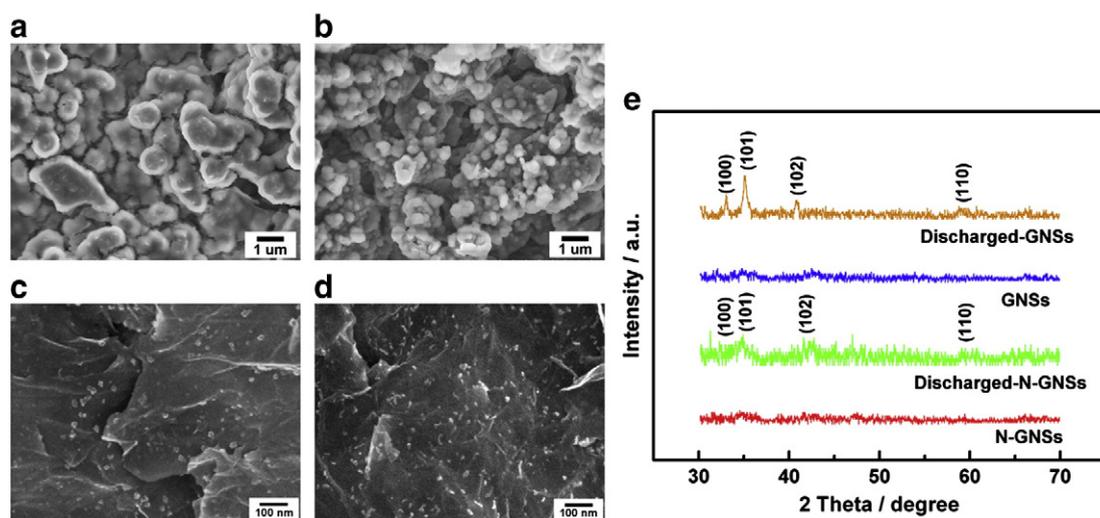
Fig. 3. SEM images of the fully discharged a, GNSs, b, N-GNSs electrodes and c, GNSs, d, N-GNSs electrodes discharged for 1 h; e, XRD patterns of pristine and discharged GNSs and N-GNSs electrodes.

defects after nitrogen doping [21]. There are more defects and functional groups after nitrogen doping, and the carbon atoms adjacent to nitrogen dopants possess higher positive charge density, resulting in an enhanced adsorption of oxygen and reactive intermediates which enhances the ORR [22].

The morphologies of discharge products for GNSs and N-GNSs electrodes are shown in Fig. 3a and b, respectively. It can be seen that the morphologies of the products on the two surfaces are significantly different. The diameter of the particles is about 600~1000 nm for GNSs and 200~500 nm for N-GNSs. Recent study by Density Functional Theory (DFT) calculations have shown that the discharge products most likely prefer to nucleate and grow around the defective sites with functional groups on GNSs [8]. To confirm it by experiment, the electrodes were discharged for 1 h and the SEM images of the products are shown in Fig. 3c and d. On GNSs, the product particle size is distributed from 20 to 45 nm, whereas on N-GNSs, a smaller size from 5 to 20 nm is observed. Moreover, the distribution of the product is more uniform on N-GNSs, while the product particles aggregated into large clusters on GNSs and some surfaces are free of coverage. These observations suggest that the presence of the homogeneously distributed nitrogen species resulting in more active sites (defects and functional groups) of N-GNSs provides more nucleation sites and thus promotes a higher dispersion. The GNSs and N-GNSs electrodes before and after discharge were examined by XRD and the patterns are shown in Fig. 3e. The additional peaks of both electrodes after discharge were assigned to Li_2O_2, whereas neither Li_2O nor Li_2CO_3 was detected, and the results are consistent with the formation of Li_2O_2 obtained by other groups [23]. It is important to note that the peaks of the products of N-GNSs electrodes were broader than those of GNSs electrodes, which may be due to the smaller crystallite sizes of Li_2O_2, consistent with the SEM results discussed above.

4. Conclusions

The performance improvement of N-GNSs as cathode materials for lithium-oxygen batteries is due to the defects and functional groups introduced by nitrogen doping. More importantly, for the first time, we showed that the catalytic activity for ORR of N-GNSs in a nonaqueous electrolyte is much higher than that of GNSs. This finding gives a rational direction to modify other carbon materials for application in lithium-oxygen batteries.

References

[1] K. Abraham, Z. Jiang, Journal of the Electrochemical Society 143 (1996) 1.
[2] G. Girishkumar, B. McCloskey, A.C. Luntz, S. Swanson, W. Wilcke, Journal of Physical Chemistry Letters 1 (2010) 2193.
[3] R.E. Williford, J.-G. Zhang, Journal of Power Sources 194 (2009) 1164.
[4] C. Trana, X.-Q. Yang, D. Qu, Journal of Power Sources 195 (2010) 2057.
[5] R.R. Mitchell, B.M. Gallant, C.V. Thompson, Y. Shao-Horn, Energy & Environmental Science 4 (2011) 2952.
[6] Y. Li, J. Wang, X. Li, D. Geng, R. Li, X. Sun, Chemical Communications 47 (2011) 9438.
[7] E. Yoo, H. Zhou, ACS Nano 5 (2011) 3020.
[8] J. Xiao, D. Mei, X. Li, W. Xu, D. Wang, G. Graff, W. Bennett, Z. Nie, L. Saraf, I. Aksay, J. Liu, J.-G. Zhang, Nano Letters 11 (2011) 5071.
[9] L. Qu, Y. Liu, J.-B. Baek, L. Dai, ACS Nano 4 (2010) 1321.
[10] X. Li, D. Geng, Y. Zhang, X. Meng, R. Li, X. Sun, Electrochemistry Communications 13 (2011) 822.
[11] D. Geng, S. Yang, Y. Zhang, J. Yang, J. Liu, R. Li, T.-K. Sham, X. Sun, S. Ye, S. Knights, Applied Surface Science 257 (2011) 9193.
[12] P. Kichambare, J. Kumar, S. Rodrigues, B. Kumar, Journal of Power Sources 196 (2010) 3310.
[13] Y. Li, J. Wang, X. Li, J. Liu, D. Geng, J. Yang, R. Li, X. Sun, Electrochemistry Communications 13 (2011) 668.
[14] Y.-C. Lu, H. Gasteiger, Y. Shao-Horn, Electrochemical and Solid-State Letters 14 (2011) A70.
[15] Y.-C. Lu, H. Gasteiger, Y. Shao-Horn, Journal of the American Chemical Society 133 (2011) 19048.
[16] S. Ye, A.K. Vijh, Electrochemistry Communications 5 (2003) 272.
[17] S. Wang, D. Yu, L. Dai, Journal of the American Chemical Society 133 (2011) 5182.
[18] Y.-C. Lu, H. Gasteiger, E. Crumlin, R. McGuire Jr., Y. Shao-horn, Journal of the Electrochemical Society 157 (2010) A1016.
[19] E. Yeager, Journal of Molecular Catalysis 38 (1986) 5.
[20] Y. Wang, Y. Shao, D.W. Matson, J. Li, Y. Lin, ACS Nano 4 (2010) 1790.
[21] D. Deng, X. Pan, L. Yu, Y. Cui, Y. Jiang, J. Qi, W. Li, Q. Fu, X. Ma, Q. Xue, G. Sun, X. Bao, Chemistry of Materials 23 (2011) 1188.
[22] C.V. Rao, C.R. Cabrera, Y. Ishikawa, Journal of Physical Chemistry Letters 1 (2010) 2622.
[23] Z. Peng, S. Freunberger, L. Hardwick, Y. Chen, V. Giordani, F. Bardé, P. Novák, D. Graham, J.-M. Tarascon, P. Bruce, Angewandte Chemie International Edition 50 (2011) 6351.